



Anomalous magnetotransport behavior in single-crystal VSb₂Li-Xin Gao ¹, Wei-Bin Wu,¹ Jing-Yu He,¹ Fei Chen,^{1,2} Qi-Ling Xiao,¹ and Jun-Yi Ge ^{1,2,*}¹Materials Genome Institute, Shanghai University, Shanghai 200444, China²Zhejiang Laboratory, Hangzhou 311100, China

(Received 25 October 2022; revised 15 January 2023; accepted 6 February 2023; published 13 February 2023)

We report the anomalous magnetotransport properties in high-quality single-crystal VSb₂ without V atom vacancies. VSb₂ shows typical metallic behavior with convex-upward characteristics, which can be explained using a parallel-resistor model. The three-dimensional weak antilocalization effect leads to a large saturation magnetoresistance (MR) up to 595%, which disappears when the magnetic field is along the *ab* plane. Instead, a clear Shubnikov–de Haas oscillation at low temperatures is observed, based on which the fast Fourier transformation spectrum analyses reveal three fundamental frequencies. The two-carrier fitting of Hall resistivity suggests that the saturation MR originates from the giant magnitude difference of the two carrier concentrations. Moreover, the angle-resolved magnetoresistance is measured by rotating the sample around its *c* axis and *ab* plane. A transition from twofold symmetry to isotropy is observed.

DOI: [10.1103/PhysRevB.107.085120](https://doi.org/10.1103/PhysRevB.107.085120)**I. INTRODUCTION**

Materials with nontrivial topological states have attracted much attention because of their abundant physical properties and potential for device-based applications [1–5]. Topological insulators (TIs) have the characteristic of gapless surface states protected by time-reversal symmetry and a novel quantum state with a metallic edge or surface state within the bulk band gap [6]. In topological Dirac [7–9] and Weyl [10–12] semimetals, discrete fourfold Dirac points or twofold Weyl points occur as a result of the electronic bands crossing each other in the momentum space. In addition to the topological states, some of these semimetals exhibit significant transport properties including high mobilities [13,14], an extremely large magnetoresistivity (XMR) [15,16], negative longitudinal magnetoresistivity [14,17], and an anomalous Hall effect [18,19]. Up to now, the electron-hole carrier compensation mechanism [15,20], the topological protection [3], and the open orbit condition [21] have been proposed to explain the origin of the anomalous magnetoresistivity. Moreover, the unique spin structure of the topological surface states often induces the weak antilocalization effect (WAL) due to the lack of backscattering [22]. These exotic phenomena suggest the interesting fundamentals of condensed matter physics in quantum materials.

Recently, transition-metal pnictides XPn_2 ($X = \text{V, Nb, Ta}$; $Pn = \text{P, As, Sb}$) have been found to be a new family of topological materials [23–27]. The XPn_2 -type compounds crystallize in a centrosymmetric monoclinic structure with a space group of $C12/m1$. The nonsaturation large MR reaching 2000% at 9 T and the negative longitudinal MR have been observed in the topological semimetal NbAs₂ [14]. Furthermore, single-crystal TaSb₂ [28] displays an ultrahigh carrier

mobility and anisotropic MR, implying a possible topological phase transition at a metal-insulator-like transition. Among XPn_2 compounds, single-crystal VSb₂ [29–37] holds metallic behavior even at high magnetic fields, which is different from other XPn_2 -type semimetals. It is necessary to identify the mechanisms of the unique transport behaviors in single-crystal VSb₂.

Preceding studies on single-crystal $V_{1-\delta}\text{Sb}_2$ ($\delta = 0.03, 0.04, 0.08, 0.1$) indicated that off-stoichiometric formations are more easily obtained. However, an investigation of VSb₂ without vacancies is absent. In this paper, we have grown high-quality single-crystal VSb₂ without V vacancies. The transport properties of VSb₂ are systematically investigated and anomalous magnetotransport behavior is observed. The saturation behavior of MR is quite different from the previous report [37]. Meanwhile, the three-dimensional weak antilocalization (WAL) effect in our sample is consistent with Ref. [37] and originates from strong spin-orbit coupling (SOC). Weak electron antilocalization decreases the probability of localizing an electron and is accompanied with a distinct magnetoresistance dip at low magnetic fields. Unexpected Shubnikov–de Haas (SdH) oscillations take place when the magnetic field is along the *c* axis. Moreover, the observed anomalous Hall effect can be explained using the two-carrier model. When the magnetic field rotates in different planes, the angle-resolved magnetoresistance transits from twofold to isotropy, indicating the nontrivial electric transport behaviors of single-crystal VSb₂.

II. EXPERIMENTS

High-quality single-crystal VSb₂ was grown by the flux method [33]. As mentioned above, off-stoichiometric $V_{1-\delta}\text{Sb}_2$ crystals have been grown in previous reports. To get VSb₂ without V vacancy, we have modified the growing conditions as follows: High-purity powders of V (99.9%) and Sb

*junyi_ge@t.shu.edu.cn

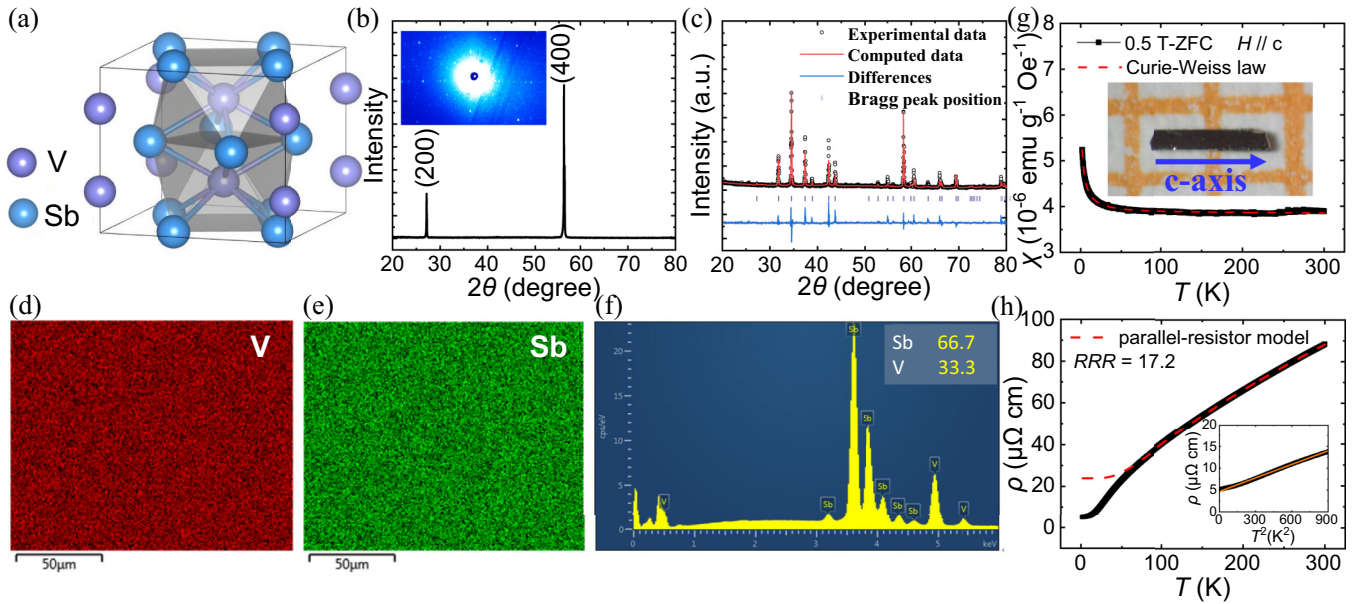


FIG. 1. (a) Crystal structure of VSb_2 . (b) X-ray diffraction pattern of single-crystal VSb_2 , showing only $(J00)$ reflection. (c) Powder XRD patterns of single-crystal VSb_2 . (d), (e) Element distribution diagram of the elements V and Sb. (f) Energy-dispersive x-ray spectroscopy of single-crystal VSb_2 . (g) $\chi(T)$ as a function of temperature for $H \parallel c$ and $\mu_0 H = 0.5$ T under the ZFC mode. The dashed line is a fitting curve of the Curie-Weiss law. Inset: Photograph of typical single-crystal VSb_2 on a 1-mm-grid paper. (h) Temperature dependence of the c -axis resistivity at zero magnetic field. The red dashed line is a fitting curve of the parallel-resistor model. Inset: T^2 dependence of the resistivity at low temperatures. The solid line is attained by linear fitting.

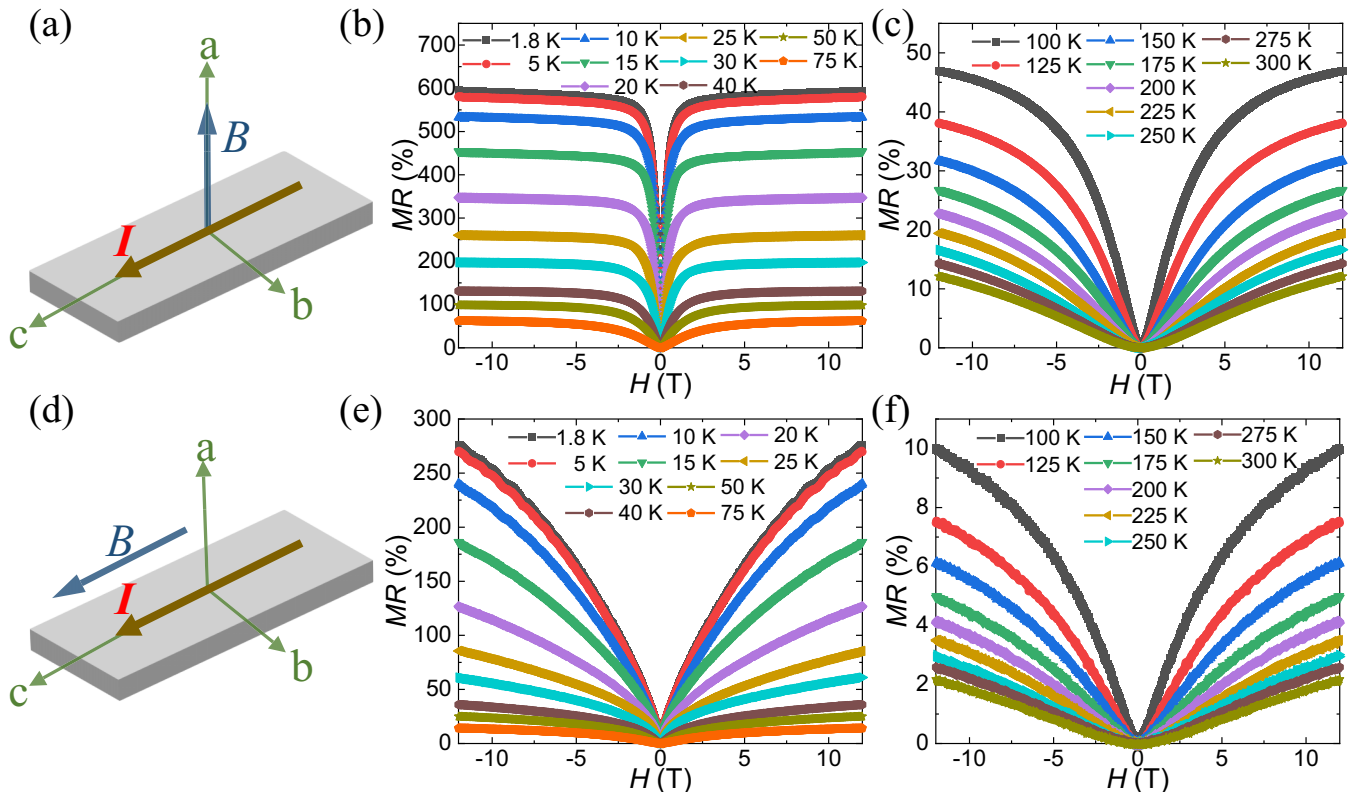


FIG. 2. (a)–(c) Transverse magnetoresistivity at different temperatures with the applied magnetic field ranging from -12 to 12 T. (d)–(f) Longitudinal magnetoresistivity at different temperatures. Clear Shubnikov–de Haas (SdH) oscillations at low temperatures and high magnetic field are observed.

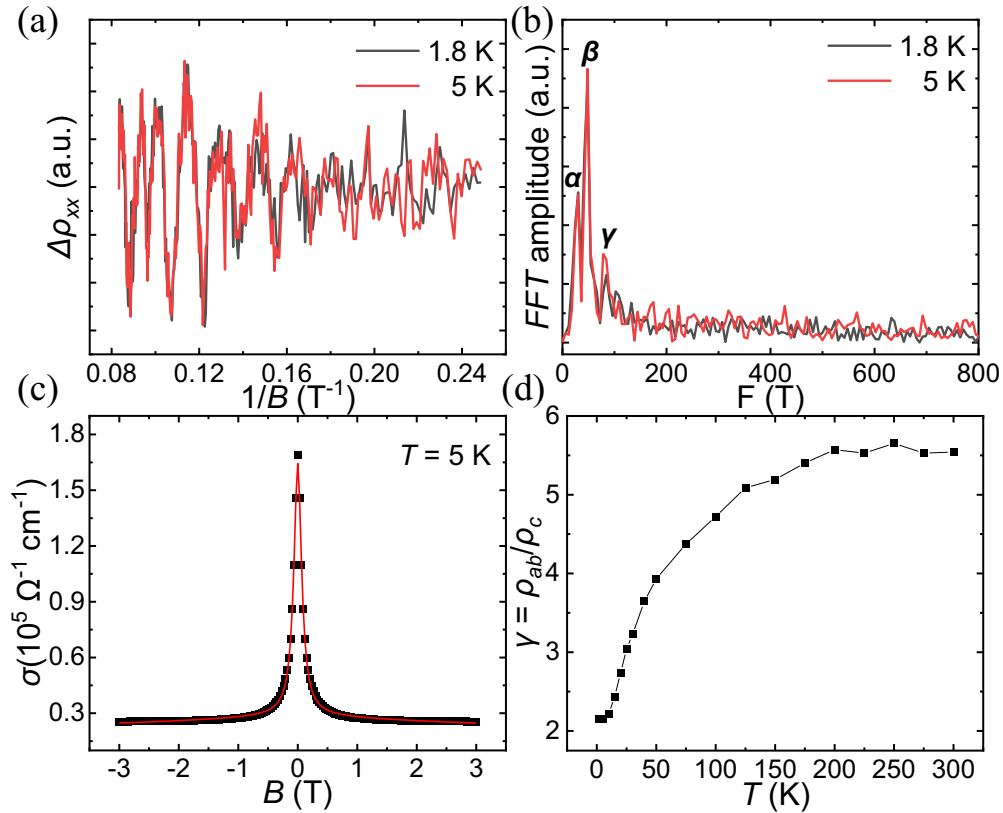


FIG. 3. (a) The oscillatory component of the resistivity $\Delta \rho_{xx}$ at 1.8 and 5 K. (b) The FFT spectrum of $\Delta \rho_{xx}$ at different temperatures. Three frequencies are extracted. (c) WAL effect in the perpendicular magnetic field at 5 K. The black circles and the red line represent the experimental data and theoretical fitting, respectively. (d) Temperature dependence of the anisotropy for single-crystal VSb₂.

(99.999%) were weighed with the molar ratio V : Sb = 1 : 5. Here, a slightly lower Sb content is used as compared with that in previous reports (e.g., 1 : 10 in Ref. [33] and 1 : 30 in Ref. [37]), which always lead to the formation of VSb₂ with V vacancies. The reactants were placed in an alumina crucible and sealed in an evacuated quartz tube. The sealed quartz tube was heated to and soaked at 1373 K for 24 h, then cooled down to 1163 K at 1.5 K/h. The slower cooling rate is chosen to make sure there is enough time for the crystal growth in our work. Finally, the quartz tube was moved quickly into the centrifuge to separate the excess Sb flux. The crystallographic orientations of single-crystal VSb₂ were determined by back-reflection Laue x-ray photography. X-ray diffraction (XRD) was performed using a Bruker D2 x-ray machine with CuK α radiation ($\lambda = 0.15418$ nm). The electric transport properties were measured using a physical property measuring system (PPMS, Quantum Design). The resistivity was measured by using a standard four-probe method. The inset of Fig. 1(h) shows an image of the as-grown single-crystal VSb₂ of size $1.5 \times 0.25 \times 0.18$ mm³. The four-probe method is used to measure the resistivity. The distance between the two voltage contacts is 0.9 mm.

III. RESULTS AND DISCUSSIONS

The crystal structure of VSb₂ was reported to be a tetragonal system with a space group of $I4/mcm$ [29,30,35]. Figure 1(a) shows the crystal structure of VSb₂ with alter-

nating stacking layers of V and Sb atoms. The XRD pattern of single-crystal VSb₂ shows only ($J00$) peaks as shown in Fig. 1(b). The inset shows the backreflection Laue images of single-crystal VSb₂ along the a axis. The bright diffraction spots suggest the high quality of the crystal. The powder XRD patterns of ground single-crystal VSb₂ are displayed in Fig. 1(c). All the diffraction peaks can be well indexed with the VSb₂ phase. Through Rietveld refinement, the weighted profile agreement factor (R_{wp}) of the Rietveld refinement is 14.6%. The refined lattice parameters are $a = 6.549$ Å, $c = 5.630$ Å. As shown in Figs. 1(d)–1(f), the homogeneous distribution of V and Sb elements has been observed with an average ratio of 1 : 2 by using energy-dispersive x-ray spectroscopy (EDS) measurements, which is different from previous reports [33,37]. No trace of V deficiency is observed. It has been reported that the atom vacancy in VSe₂ [38,39] could lead to an unexpected breakdown of magnetic order and the introduction of a local magnetic moment compared with stoichiometric compounds. It is of interest to investigate the magnetic properties of our samples and compare with the results in previous reports. Figure 1(g) shows the magnetic susceptibility $\chi(T)$ curves at $\mu_0 H = 0.5$ T with the zero-field-cooling (ZFC) mode for $H \parallel c$. The results can be well fitted with the Curie-Weiss law [37,40,41] $\chi = \chi_0 + C/(T - \theta)$, where χ_0 is the temperature-dependent susceptibility, C is the Curie constant, and θ is the Weiss temperature. The fitting results are $\chi_0 = 3.83 \times 10^{-6}$ emu g⁻¹ Oe⁻¹ and $C = 1.79 \times 10^{-3}$

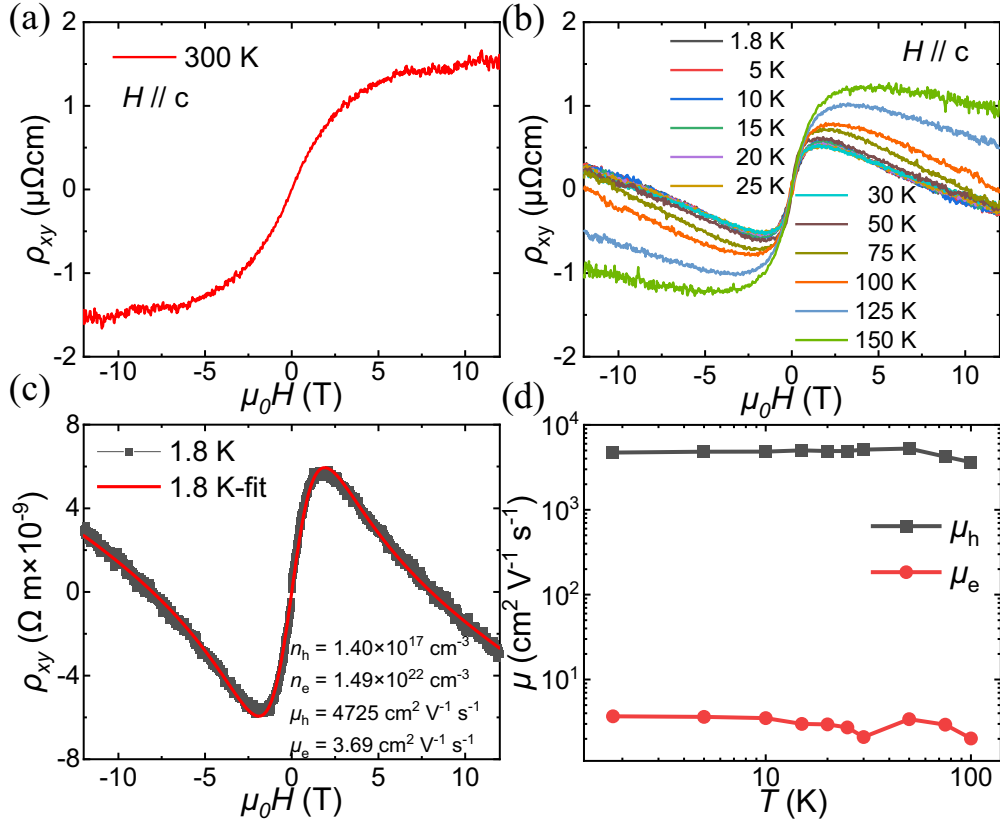


FIG. 4. (a) The magnetic field dependence of the Hall resistivity at 300 K. (b) The Hall resistivity at different temperatures from 1.8 to 150 K. (c) The nonlinear fit of the Hall resistivity at 1.8 K based on the two-carrier model. (d) Temperature dependence of carrier mobility μ_e and μ_h of electrons and holes deduced by the two-carrier model.

emu K mol^{-1} . The effective magnetic moment per formal unit has been calculated as $0.12\mu_B/\text{V}$ smaller than that in an off-stoichiometric formation. The result in this study indicates the V vacancies might induce paramagnetic moments but hardly change the magnetic structure of single-crystal VSb_2 . The determined value of $\theta = -2.5\text{ K}$ suggests the antiferromagnetic coupling between V atoms, which has been reported in a previous work. The inset of Fig. 1(g) shows an optical image of the studied crystal.

Figure 1(h) presents the temperature dependence of longitudinal resistivity in zero magnetic field. The high-quality sample shows a typical metallic behavior with the residual resistivity ratio $\text{RRR} = \rho(300\text{ K})/\rho(1.8\text{ K}) = 17.2$, higher than that in earlier reports [34,37]. The $\rho(T)$ curve exhibits convex-upward characteristics at temperatures greater than 25 K. Similar behavior has been observed in other metallic materials and can be interpreted using a parallel-resistor model [42]. The resistance reaches saturation at high temperatures when the mean free path is comparable to the order of the interatomic spacing. The parallel-resistor model can be expressed as $\frac{1}{\rho(T)} = \frac{1}{\rho_{\text{sat}}} + \frac{1}{\rho_1(T)}$, where ρ_{sat} is the resistivity saturated at high temperatures and is independent of temperature, $\rho_1(T)$ is the ideal temperature-dependent resistivity dominated by the electron-phonon scattering according to the Matthiessen's rule. $\rho_1(T) = \rho_0 + A\left(\frac{T}{\theta_D}\right)^5 \int_0^{\frac{T}{\theta_D}} \frac{x^5}{[\exp(x)-1][1-\exp(-x)]}$, where ρ_0 is the residual

resistivity caused by impurity scattering and disorder, A is a numerical constant, and θ_D is the Debye temperature. The data for ρ from 300 to 60 K were fitted to this model as the red dashed line in Fig. 1(h), which yields $\rho_{\text{sat}} = 461.4\ \mu\Omega\text{ cm}$, residual resistivity $= 25.1\ \mu\Omega\text{ cm}$, $A = 353.2\ \mu\Omega\text{ cm}$, and Debye temperature $\theta_D = 298.8\text{ K}$. However, the resistivity is proportional to T^2 at low temperatures [Fig. 1(h) inset], which might arise from an increase of the disorder [43].

The samples without V atom vacancies grow along the c axis and have a stronger metallic property. In order to compare the magnetotransport behaviors with that of $\text{V}_{1-\delta}\text{Sb}_2$ [37], a systematic magnetoresistance measurement was carried out. Figure 2 shows the magnetoresistance measured from 1.8 to 300 K with the electric current $I \parallel c$ axis. As shown in Figs. 2(a)–2(c), the transverse MR increases rapidly and then saturates at high magnetic fields and low temperatures. The value at 1.8 K and 12 T reaches up to 595% larger than the reported value of 447% [37]. Furthermore, this saturation behavior of MR is quite different from the reported MR curves with the electric current $I \parallel ab$ plane. With increasing temperature, the saturation value of MR becomes smaller and the saturation field shifts to higher values. This evolution of MR can be explained within the framework of a two-band model [44]. The saturation MR occurs when one type of carrier has a much higher concentration than the other type. Meanwhile, at higher temperatures, the saturation behavior shifts to higher field values with the decrease of the carrier mobility μ . As

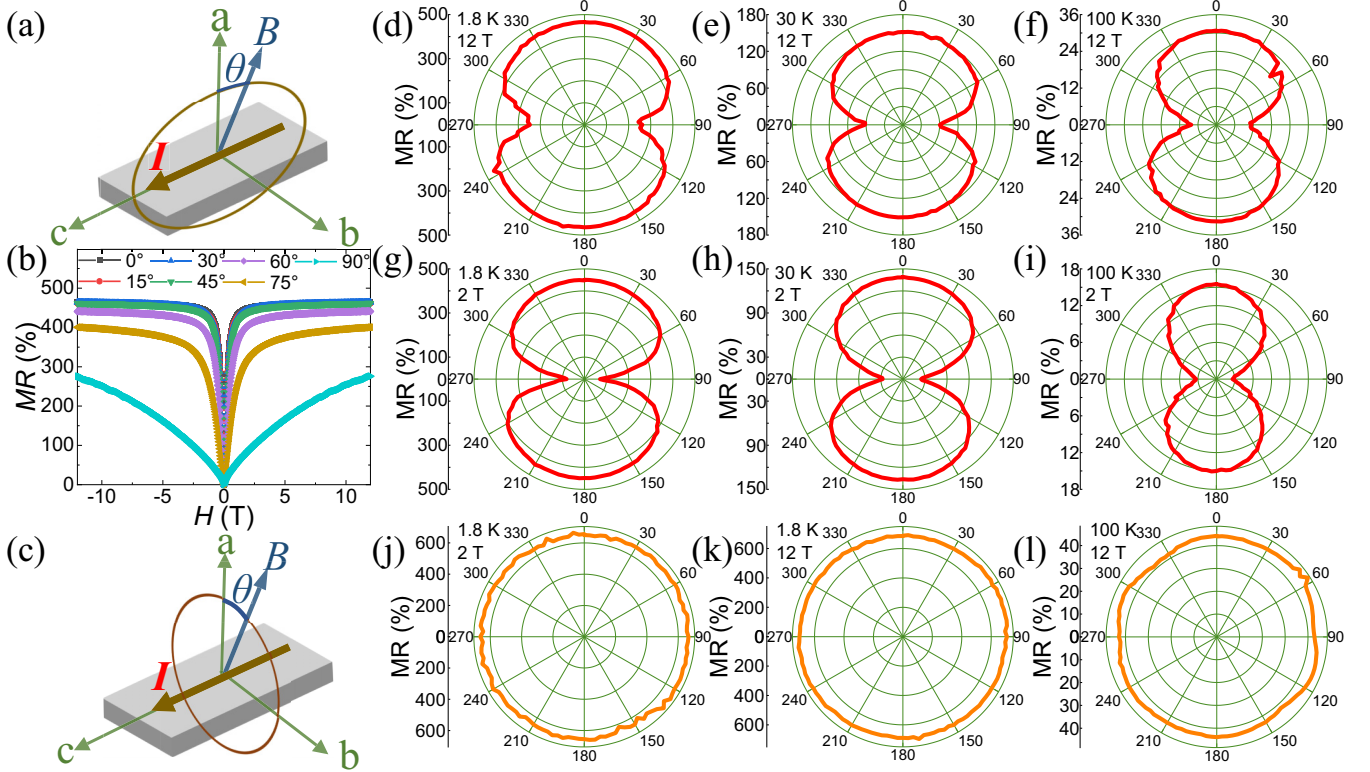


FIG. 5. (a), (c) Schematic of the experimental configuration for AMR in the ac and ab planes, respectively. (b) Magnetoresistance with applied field from perpendicular ($\theta = 0^\circ$) to parallel ($\theta = 90^\circ$) to the electric current at 1.8 K. (d)–(i) Polar plots illustrating the twofold AMR effect in the ac plane under 2 and 12 T at several temperatures. (j)–(l) Polar plots illustrating the isotropic AMR in the ab plane.

shown in Figs. 2(d)–2(f), the saturation behavior of longitudinal MR can no longer be observed. The longitudinal MR increases gradually with magnetic field and reaches 276% at 1.8 K and 12 T. Moreover, it is astonishing to observe the SdH oscillations under low temperatures and high magnetic fields.

The investigation on the SdH oscillations has proven to be effective for studying topologically nontrivial transport properties. Figure 3(a) shows the oscillation of $\Delta\rho_{xx}$ against the reciprocal of the magnetic field $1/B$ by subtracting a smoothed polynomial background. To confirm the oscillation frequencies and obtain more information about the Fermi surface, the fast Fourier transformation (FFT) spectrum of $\Delta\rho_{xx}$ is taken as shown in Fig. 3(b). Three fundamental frequencies can be identified clearly, which are labeled as F_α (30.6 T), F_β (48.5 T), and F_γ (80.4 T). According to the Onsager relation $F = (\phi_0/2\pi^2)A = (\hbar/2\pi e)A$, the frequency F is proportional to the cross section of the Fermi surface. We observe the extremal Fermi surface area $S_\alpha = 2.96 \times 10^{-3} \text{ \AA}^{-2}$, $S_\beta = 4.69 \times 10^{-3} \text{ \AA}^{-2}$, and $S_\gamma = 7.78 \times 10^{-3} \text{ \AA}^{-2}$.

Furthermore, we note that the MR curve in Fig. 2(b) exhibits an obvious WAL effect. The WAL effect is generally observed in topological materials due to the generation of a nontrivial band, which is closely related to strong spin-orbit coupling [45–47]. The effect of WAL on transport properties can be described using the formula [22,48]

$$\sigma(B) = \sigma_{\text{WAL}} + \sigma_N, \quad (1)$$

where

$$\sigma_{\text{WAL}} = \sigma_0 + a\sqrt{B}, \quad (2)$$

$$\sigma_N^{-1} = \rho_0 + A \cdot B^2. \quad (3)$$

σ_0 is the zero-field conductivity, and a and A are numerical constants. σ_{WAL} and σ_N are those from the WAL effect and conventional nonlinear band contributions around the Fermi level, respectively. Figure 3(c) presents the magnetic field dependence of the conductivity σ . The fitting yields the parameters of $\sigma_0 = 3.1 \times 10^5 \text{ \Omega}^{-1} \text{ cm}^{-1}$, $\rho_0 = 7.5 \times 10^{-6} \text{ \Omega cm}$. The three-dimensional WAL effect of our sample is consistent with the result in $\text{V}_{1-\delta}\text{Sb}_2$ [37]. The estimated anisotropy $\gamma = \rho_{ab}/\rho_c$ is shown in Fig. 3(d). γ increases with temperature until saturation at 200 K.

The saturation magnetoresistance and quantum oscillatory results reported here, and the samples in this paper exhibit different properties from $\text{V}_{1-\delta}\text{Sb}_2$, which suggest that the V atom vacancies have a significant effect on the transport properties of single crystals. To learn more about the origin of the anomalous magnetotransport behaviors in single-crystal VSb_2 , the Hall resistivity was measured. Figure 4(a) shows the magnetic field dependence of the Hall resistivity at 300 K. The observed nonlinear Hall curve is a characteristic of two-carrier transport. The positive slope in high magnetic fields indicates that holes dominate the transport processes. The magnetic field dependence of the Hall resistivity at low temperatures is presented in Fig. 4(b). Contrary to the result

of 300 K, the slopes are negative in high magnetic fields, implying that the electron-dominated conduction transforms to a hole type with an increase of temperature. The values of the carrier densities and mobilities have been estimated by fitting the experimental data with a two-carrier model [49,50],

$$\rho_{xy} = \frac{1}{e} \frac{(n_h \mu_h^2 - n_e \mu_e^2) + \mu_h^2 \mu_e^2 B^2 (n_h - n_e)}{(n_h \mu_h + n_e \mu_e)^2 + \mu_h^2 \mu_e^2 B^2 (n_h - n_e)^2} B, \quad (4)$$

where n_e (n_h) and μ_e (μ_h) are the carrier density and mobility of electrons (holes), respectively. The fitting result at 1.8 K is shown in Fig. 4(c), which yields carrier densities of $n_h = 1.40 \times 10^{17} \text{ cm}^{-3}$ and $n_e = 1.49 \times 10^{22} \text{ cm}^{-3}$, with corresponding carrier mobilities of $\mu_h = 4725 \text{ cm}^2 \text{ V}^{-1} \text{ s}^{-1}$ and $\mu_e = 3.69 \text{ cm}^2 \text{ V}^{-1} \text{ s}^{-1}$. The error has been observed in the fitting result of the hole concentrations but it does not affect other parameters. Therefore, we compared the carrier mobilities of holes and electrons from 1.8 to 100 K in Fig. 4(d). The value of carrier mobility for holes is three orders of magnitude greater than that for electrons. The hole carriers with larger mobilities might be one of the reasons for the generation of a large MR. Meanwhile, the giant magnitude difference of the two carrier concentrations is consistent with the appearance of the saturation MR in Fig. 2(a) mentioned above.

To further investigate the anisotropy of VSb₂, angle-resolved magnetoresistance (AMR) is measured by rotating the sample around its *c* axis and *ab* plane. The electric current was applied along the *c* axis during the measurements. As shown in Fig. 5(b), the MR is measured by tilting the magnetic field from perpendicular ($\theta = 0^\circ$) to parallel ($\theta = 90^\circ$) to the electric current direction at 1.8 K. As the angle increases, the magnetic field component, perpendicular to the current, decreases and the anisotropy becomes larger. The disappearance of the MR saturation under the parallel magnetic field might be related to the anisotropy of the carrier mobility. The results of the AMR under 2 and 12 T at various temperatures are presented with a polar plot. As seen in Figs. 5(d)–5(i), when the magnetic field rotates in the *ac* plane, AMR retains a twofold symmetry in the whole temperature range, and becomes more anisotropic at low magnetic fields and high temperatures. In contrast, the AMR evolves into isotropic when the magnetic field is perpendicular to the current in Figs. 5(j)–5(l). The

possible origin of the circular AMR is the concealment of the *C*₄ rotational symmetry determined by the crystal structure, because of the large magnetoresistance effect induced by the WAL effect. The symmetry, corresponding to a mixed state with a dominant twofold symmetry at low magnetic fields, becomes fourfold and eightfold under high magnetic fields in Ag₃Sn [51]. In our samples, the MR increases rapidly and then saturates due to the WAL effect. The twofold symmetry is covered by the magnetoresistance effect, which should play a dominant role at low magnetic fields. In addition, the angle-resolved magnetoresistance features also possibly result from a topological band feature. When the magnetic field rotates in the *ac* plane, twofold symmetry shows up due to the changes of the angle between the magnetic field and current. More research is needed to further verify this issue.

IV. CONCLUSION

In summary, we grew high-quality single-crystal VSb₂ and conducted systematic magnetotransport measurements. Large saturation magnetoresistance (MR) approaches 595% under perpendicular magnetic fields. The observed three-dimensional WAL effect implies strong spin-orbit coupling in single-crystal VSb₂. In addition, SdH oscillations are observed under low temperature at high magnetic fields when a parallel magnetic field is applied. The analysis of the Hall effect reveals the transformation from an electron-dominated conduction mechanism to a hole-type mechanism with an increase of temperature. In addition, the transition of AMR from twofold symmetry to isotropy implies nontrivial transport properties.

ACKNOWLEDGMENTS

The study was supported by the National Key Research and Development Program of China (Grant No. 2018YFA0704300) and the National Natural Science Foundation of China (Grants No. 12174242 and No. 11804217). J.-Y.G. is also thankful for support by the Program for Professor of Special Appointment (Eastern Scholar) at Shanghai Institutions of Higher Learning.

[1] X. L. Qi and S. C. Zhang, Topological insulators and superconductors, *Rev. Mod. Phys.* **83**, 1057 (2011).
 [2] Z. Wang, Y. Sun, X.-Q. Chen, C. Franchini, G. Xu, H. Weng, X. Dai, and Z. Fang, Dirac semimetal and topological phase transitions in *A*₃Bi (*A* = Na, K, Rb), *Phys. Rev. B* **85**, 195320 (2012).
 [3] T. Liang, Q. Gibson, M. N. Ali, M. Liu, R. Cava, and N. Ong, Ultrahigh mobility and giant magnetoresistance in the Dirac semimetal Cd₃As₂, *Nat. Mater.* **14**, 280 (2015).
 [4] J. Hu, Y. L. Zhu, D. Graf, Z. J. Tang, J. Y. Liu, and Z. Q. Mao, Quantum oscillation studies of the topological semimetal candidate ZrGeM (*M* = S, Se, Te), *Phys. Rev. B* **95**, 205134 (2017).
 [5] Y. Y. Lv, B. B. Zhang, X. Li, K. W. Zhang, X. B. Li, S. H. Yao, Y. B. Chen, J. Zhou, S. T. Zhang, M. H. Lu, S. C. Li, and

Y. F. Chen, Shubnikov–de Haas oscillations in bulk ZrTe₅ single crystals: Evidence for a weak topological insulator, *Phys. Rev. B* **97**, 115137 (2018).
 [6] M. Z. Hasan and C. L. Kane, Colloquium: Topological insulators, *Rev. Mod. Phys.* **82**, 3045 (2010).
 [7] S. M. Young, S. Zaheer, J. C. Y. Teo, C. L. Kane, E. J. Mele, and A. M. Rappe, Dirac Semimetal in Three Dimensions, *Phys. Rev. Lett.* **108**, 140405 (2012).
 [8] Z. Liu, B. Zhou, Y. Zhang, Z. Wang, H. Weng, D. Prabhakaran, S.-K. Mo, Z. Shen, Z. Fang, X. Dai, Z. Hussain, and Y. L. Chen, Discovery of a three-dimensional topological dirac semimetal, Na₃Bi, *Science* **343**, 864 (2014).
 [9] J. Feng, Y. Pang, D. Wu, Z. Wang, H. Weng, J. Li, X. Dai, Z. Fang, Y. Shi, and L. Lu, Large linear magnetoresistance in

- Dirac semimetal Cd_3As_2 with Fermi surfaces close to the Dirac points, *Phys. Rev. B* **92**, 081306(R) (2015).
- [10] G. Xu, H. M. Weng, Z. J. Wang, X. Dai, and Z. Fang, Chern Semimetal and the Quantized Anomalous Hall Effect in HgCr_2Se_4 , *Phys. Rev. Lett.* **107**, 186806 (2011).
- [11] H. Weng, C. Fang, Z. Fang, B. A. Bernevig, and X. Dai, Weyl Semimetal Phase in Noncentrosymmetric Transition-Metal Monophosphides, *Phys. Rev. X* **5**, 011029 (2015).
- [12] L. Huang, T. M. McCormick, M. Ochi, Z. Zhao, M.-T. Suzuki, R. Arita, Y. Wu, D. Mou, H. Cao, J. Yan, N. Trivedi, and A. Kaminski, Spectroscopic evidence for a type II Weyl semimetallic state in MoTe_2 , *Nat. Mater.* **15**, 1155 (2016).
- [13] C. Shekhar, A. K. Nayak, Y. Sun, M. Schmidt, M. Nicklas, I. Leermakers, U. Zeitler, Z. K. Liu, Y. L. Chen, W. Schnelle, J. Grin, C. Felser, and B. Yan, Extremely large magnetoresistance and ultrahigh mobility in the topological Weyl semimetal candidate NbP , *Nat. Phys.* **11**, 645 (2015).
- [14] B. Shen, X. Y. Deng, G. Kotliar, and N. Ni, Fermi surface topology and negative longitudinal magnetoresistance observed in the semimetal NbAs_2 , *Phys. Rev. B* **93**, 195119 (2016).
- [15] Z. W. Zhu, X. Lin, J. Liu, B. Fauqué, Q. Tao, C. L. Yang, Y. G. Shi, and K. Behnia, Quantum Oscillations, Thermoelectric Coefficients, and the Fermi Surface of Semimetallic WTe_2 , *Phys. Rev. Lett.* **114**, 176601 (2015).
- [16] L. X. Zhao, L. C. Xu, H. K. Zuo, X. M. Wu, G. Y. Gao, and Z. W. Zhu, Fermi surface and carrier compensation of pyrite-type PtBi_2 revealed by quantum oscillations, *Phys. Rev. B* **98**, 085137 (2018).
- [17] Z. J. Yuan, H. Lu, Y. J. Liu, J. F. Wang, and S. Jia, Large magnetoresistance in compensated semimetals TaAs_2 and NbAs_2 , *Phys. Rev. B* **93**, 184405 (2016).
- [18] K. Y. Yang, Y. M. Lu, and Y. Ran, Quantum Hall effects in a Weyl semimetal: Possible application in pyrochlore iridates, *Phys. Rev. B* **84**, 075129 (2011).
- [19] E. K. Liu, Y. Sun, N. Kumar, L. Muechler, A. L. Sun, L. Jiao, S. Y. Yang, D. F. Liu, A. J. Liang, Q. N. Xu, J. Kroder, V. Süß, H. Borrmann, C. Shekhar, Z. S. Wang, C. Y. Xi, W. H. Wang, W. Schnelle, S. Wirth, S. T. B. Goennenwein, and C. Felser, Giant anomalous Hall effect in a ferromagnetic kagome-lattice semimetal, *Nat. Phys.* **14**, 1125 (2018).
- [20] M. N. Ali, J. Xiong, S. Flynn, J. Tao, Q. D. Gibson, L. M. Schoop, T. Liang, N. Haldolaarachchige, M. Hirschberger, N. P. Ong and R. J. Cava, Large, non-saturating magnetoresistance in WTe_2 , *Nature (London)* **514**, 205 (2014).
- [21] S. N. Zhang, Q. S. Wu, Y. Liu, and O. V. Yazyev, Magnetoresistance from Fermi surface topology, *Phys. Rev. B* **99**, 035142 (2019).
- [22] X. C. Huang, L. X. Zhao, Y. J. Long, P. P. Wang, D. Chen, Z. H. Yang, H. Liang, M. Q. Xue, H. M. Weng, Z. Fang, X. Dai, and G. F. Chen, Observation of the Chiral-Anomaly-Induced Negative Magnetoresistance in 3D Weyl Semimetal TaAs , *Phys. Rev. X* **5**, 031023 (2015).
- [23] D. Wu, J. Liao, W. Yi, X. Wang, P. Li, H. Weng, Y. Shi, Y. Li, J. Luo, X. Dai, and Z. Fang, Giant semiclassical magnetoresistance in high mobility TaAs_2 semimetal, *Appl. Phys. Lett.* **108**, 042105 (2016).
- [24] Y. Li, L. Li, J. Wang, T. Wang, X. Xu, C. Xi, C. Cao, and J. Dai, Resistivity plateau and negative magnetoresistance in the topological semimetal TaSb_2 , *Phys. Rev. B* **94**, 121115(R) (2016).
- [25] C. L. Zhang, Z. J. Yuan, Q. D. Jiang, B. B. Tong, C. Zhang, X. C. Xie, and S. Jia, Electron scattering in tantalum monoarsenide, *Phys. Rev. B* **95**, 085202 (2017).
- [26] H. Wang, H. Su, J. Zhang, W. Xia, Y. Lin, X. Liu, X. Hou, Z. Yu, N. Yu, X. Wang, Z. Zou, Y. Wang, Q. Liang, Y. Zhen, and Y. Guo, Quantum oscillations and nontrivial topological state in a compensated semimetal TaP_2 , *Phys. Rev. B* **100**, 115127 (2019).
- [27] S. Chen, Z. Lou, Y. Zhou, Q. Chen, B. Xu, C. Wu, J. Du, J. Yang, H. Wang, and M. Fang, Magnetoresistance and Kondo Effect in Nodal-Line Semimetal VAs_2 , *Chin. Phys. Lett.* **38**, 017202 (2021).
- [28] X. Y. Liu, J. L. Wang, W. You, T. T. Wang, H. Y. Yang, W. H. Jiao, H. Y. Mao, L. Zhang, J. Cheng, and Y. K. Li, Anisotropic Magnetoresistivity in Semimetal TaSb_2 , *Chin. Phys. Lett.* **34**, 127501 (2017).
- [29] H. Nowotny, R. Funk, and J. Pesl, Kristallchemische Untersuchungen in den Systemen Mn-As, V-Sb, Ti-Sb, *Monatsh. Chem.* **82**, 513 (1951).
- [30] H. Nowotny and J. Pesl, Untersuchungen im System Titan—Antimon, *Monatsh. Chem.* **82**, 336 (1951).
- [31] E. E. Havinga, H. Damsma, and P. Hokkelling, Compounds and pseudo-binary alloys with the $\text{CuAl}_2(\text{C16})$ -type structure I. Preparation and x-ray results, *J. Less-Common Met.* **27**, 169 (1972).
- [32] J. D. Donaldson, A. Kjekshus, D. G. Nicholson, and T. J. Rakke, Properties of TiSb_2 and VSb_2 , *J. Less-Common Met.* **41**, 255 (1975).
- [33] M. Armbrüster, W. Schnelle, U. Schwarz, and Y. Grin, Chemical bonding in TiSb_2 and VSb_2 : A quantum chemical and experimental study, *Inorg. Chem.* **46**, 6319 (2007).
- [34] F. Failamani, P. Broz, D. Maccio, S. Puchegger, H. Müller, L. Salamakha, H. Michor, A. Grytsiv, A. Saccone, E. Bauer, G. Giester, and P. Rogl, Constitution of the systems $\{\text{V}, \text{Nb}, \text{Ta}\}\text{Sb}_2$ and physical properties of di-antimonides $\{\text{V}, \text{Nb}, \text{Ta}\}\text{Sb}_2$, *Intermetallics* **65**, 94 (2015).
- [35] S. Malki and L. El Farh, Structural and electronic properties of VSb_2 and FeSb_2 , *Mater. Today: Proc.* **13**, 991 (2019).
- [36] S. Malki and L. El Farh, First-principles investigation on thermoelectric properties of VSb_2 material, *Int. J. Thermophys.* **41**, 58 (2020).
- [37] Y. Zhang, X. L. Huang, J. L. Zhang, W. S. Gao, X. D. Zhu, and L. Pi, Intrinsic V vacancy and large magnetoresistance in $\text{V}_{1-\delta}\text{Sb}_2$ single crystal, *Chin. Phys. B* **31**, 037102 (2022).
- [38] H. Mutka and P. Molinier, Irradiation-induced defects in layered dichalcogenides: The case of VSe_2 , *J. Phys. C: Solid State Phys.* **15**, 6305 (1982).
- [39] A. O. Fumega, M. Gobbi, P. Dreher, W. Wan, C. González-Orellana, M. Peña-Díaz, C. Rogero, J. Herrero-Martín, P. Gargiani, M. Ilyn, M. M. Ugeda, V. Pardo, and S. Blanco-Canosa, Absence of ferromagnetism in VSe_2 caused by its charge density wave phase, *J. Phys. Chem. C* **123**, 27802 (2019).
- [40] A. M. Stewart, Paramagnetic susceptibilities of metallic samarium compounds, *Phys. Rev. B* **6**, 1985 (1972).
- [41] N. S. Sangeetha, V. K. Anand, Eduardo Cuervo-Reyes, V. Smetana, A.-V. Mudring, and D. C. Johnston, Enhanced moments of Eu in single crystals of the metallic helical antiferromagnet $\text{EuCo}_{2-y}\text{As}_2$, *Phys. Rev. B* **97**, 144403 (2018).

- [42] H. Wiesmann, M. Gurvitch, H. Lutz, A. Ghosh, B. Schwarz, M. Strongin, P. Allen, and J. Halley, Simple Model for Characterizing the Electrical Resistivity in A-15 Superconductors, *Phys. Rev. Lett.* **38**, 782 (1977).
- [43] M. Gurvitch, Universal Disorder-Induced Transition in the Resistivity Behavior of Strongly Coupled Metals, *Phys. Rev. Lett.* **56**, 647 (1986).
- [44] A. B. Pippard, *Magnetoresistance in Metals* (Cambridge University Press, Cambridge, U.K., 1989).
- [45] J. Chen, H. J. Qin, F. Yang, J. Liu, T. Guan, F. M. Qu, G. H. Zhang, J. R. Shi, X. C. Xie, C. L. Yang, K. H. Wu, Y. Q. Li, and L. Lu, Gate-Voltage Control of Chemical Potential and Weak Antilocalization in Bi₂Se₃, *Phys. Rev. Lett.* **105**, 176602 (2010).
- [46] M. H. Liu, J. S. Zhang, C. Z. Chang, Z. C. Zhang, X. Feng, K. Li, K. He, L. L. Wang, X. Chen, X. Dai, Z. Fang, Q. K. Xue, X. C. Ma, and Y. Y. Wang, Crossover between Weak Antilocalization and Weak Localization in a Magnetically Doped Topological Insulator, *Phys. Rev. Lett.* **108**, 036805 (2012).
- [47] S. Ishiwata, Y. Shiomi, J. Lee, M. S. Bahramy, T. Suzuki, M. Uchida, R. Arita, Y. Taguchi, and Y. Tokura, Extremely high electron mobility in a phonon-glass semimetal, *Nat. Mater.* **12**, 512 (2013).
- [48] H. J. Kim, K. S. Kim, J. F. Wang, M. Sasaki, N. Satoh, A. Ohnishi, M. Kitaura, M. Yang, and L. Li, Dirac versus Weyl Fermions in Topological Insulators: Adler-Bell-Jackiw Anomaly in Transport Phenomena, *Phys. Rev. Lett.* **111**, 246603 (2013).
- [49] P. M. C. Rourke, A. F. Bangura, C. Proust, J. Levallois, N. Doiron-Leyraud, D. LeBoeuf, L. Taillefer, S. Adachi, M. L. Sutherland, and N. E. Hussey, Fermi-surface reconstruction and two-carrier model for the Hall effect in YBa₂Cu₄O₈, *Phys. Rev. B* **82**, 020514(R) (2010).
- [50] C. Z. Li, J. G. Li, L. X. Wang, L. Zhang, J. M. Zhang, D. P. Yu, and Z. M. Liao, Two-carrier transport induced Hall anomaly and large tunable magnetoresistance in Dirac semimetal Cd₃As₂ nanoplates, *ACS Nano* **10**, 6020 (2016).
- [51] N. Zhou, Y. Sun, Q. Xu, C. Y. Xi, Z. S. Wang, B. Li, J. J. Feng, L. Zhang, X. Z. Xing, Y. F. Zhang, Y. Q. Pan, Y. Meng, X. L. Yi, L. Pi, X. Xu, and Z. Shi, Quantum oscillations and anomalous angle-dependent magnetoresistance in the topological candidate Ag₃Sn, *Phys. Rev. B* **101**, 245102 (2020).